sciendo

VOLUME 17, N° 4 2023
Journal of Automation, Mobile Robotics and Intelligent Systems

Simulation Research of Motion of Lightweight Wheeled Mobile Robot on Various Types of Soft Ground – a Case Study

Submitted: 13th October 2023; accepted: 27th November 2023

Maciej Trojnacki, Przemysław Dąbek

DOI: 10.14313/JAMRIS/4-2023/26

Abstract:
A problem of influence of three types of soft ground on longitudinal motion of a lightweight four-wheeled mobile robot is considered. Kinematic structure, main design features of the robot and its dynamics model are described. A numerical model was elaborated to simulate the dynamics of the robot's multi-body system and the wheel-ground interaction, taking into account the soil deformation and stresses occurring on the circumference of the wheel in the area of contact with the deformable ground. Numerical analysis involving four velocities of robot motion and three cases of soil (dry sand, sandy loam, clayey soil) is performed. Within simulation research, the motion parameters of the robot, ground reaction forces and moments of force, driving torques, wheel sinkage and slip parameters of wheels were calculated. Aggregated research results as well as detailed results of selected simulations are shown and discussed. As a result of the research, it was noticed that wheel slip ratios, wheels' sinkage and wheel driving torques increase with desired velocity of motion. Moreover, it was observed that wheels' sinkage and driving torques are significantly larger for dry sand than for the other investigated ground types.

Keywords: *Lightweight wheeled mobile robot, Longitudinal motion, Deformable ground, Dynamics model, Tire-ground interaction, Wheel slip, Wheel sinkage, Simulation studies*

1. Introduction

Lightweight wheeled mobile robots are versatile vehicles that work in both indoor and outdoor environments. The largest group of such vehicles are lightweight mobile robots, an example of which are robots for special applications. Such robots move on a variety of surfaces, both paved [1] and unpaved [2].

At the stage of designing robot structures and control systems, it is beneficial to know the robot dynamics model [3,4]. The form of the robot dynamics model is fundamentally influenced by its kinematic structure [5], which depends on the area of application of the robot. Such a model can be developed using classical methods, e.g., using the Newton-Euler formalism or Lagrange formalism [6].

Alternative methods may also be used in which the dynamics model can be built using system identification through measurements of the input and output signals of the system [7]. This process can be carried out both offline [8] and online, depending on the method. It also may or may not require the knowledge of the robot's model structure. Artificial intelligence methods can also be used [9], e.g., based on artificial neural networks [10], to approximate unknown nonlinear functions in the dynamics model.

Regardless of the adopted method of creating the dynamics model, it is important that it takes into account the wheel-ground interaction. For this purpose, tire models are introduced in the dynamics model. Tire-ground interaction in the case of lightweight mobile robots moving at relatively high speeds should take into account the possibility of wheel slippage. If robot motion occurs on deformable ground, then in addition to wheel slip the ground deformation has to be considered as well. Modeling the interaction of wheels with unpaved ground is the subject of terramechanics, the basis of which was formulated in the work [11].

The problem of motion on deformable ground is of critical importance in the case of outdoor wheeled mobile robots used for reconnaissance in civil and military scenarios and is related to the problem of robot mobility. In this case, the questions of how the ground type and desired robot velocity affect wheel slips, soil deformation (or wheel sinkage) and driving torques should be answered. Examples of studies of motion of vehicles on deformable grounds, especially tracked and wheeled ones, are [11, 12] and [13]. The majority of works is focused on manned vehicles; however, one can also find works concerning wheeled mobile robots, for instance [14], and in particular planetary rovers [15, 16]. Heavy off-road vehicles typically use pneumatic wheels. Apart from the tread, their driving properties are determined by tire pressure, as well as wheel diameter and width. The research results in this area are described, among others, in works [11, 12]. In turn, lightweight vehicles, such as mobile robots for special applications often have non-pneumatic wheels. Therefore, in their case, the mechanical properties of the wheel fillings used are important.

The aim of this paper is to study the influence of three types of deformable ground on the motion parameters of a lightweight wheeled mobile robot during its longitudinal motion. The analysis is carried out for the robot moving with various desired velocities on three different types of soft ground, i.e., dry sand, sandy loam and clayey soil. In the present work, the numerical analysis only is presented, but a similar study with experimental verification was carried out for dry sand in paper [17]. In the present article, the issue of the interaction of the wheel with the soft ground is also described in more detail. In particular, the distribution on the wheel circumference of soil deformations and stresses in the contact area of the wheel with the ground is analyzed, which is very difficult to perform at the stage of experimental research.

2. Robot and Its Model

Within this paper, the PIAP GRANITE four-wheeled mobile robot with non-steered wheels is analyzed. The robot's wheels are non-pneumatic, i.e., they are filled with stiffening foam. This robot is a platform dedicated to research (Fig. 1a). The robot's kinematic structure is illustrated in Figure 1b, where the particular subsystems are distinguished, i.e.: 0 – body, 1–4 – wheels, 5–6 – optional toothed belts.

The robot can be configured to work in several versions, i.e.: 1. the front or rear drive can be decoupled and only the remaining wheels can be driven; 2. only the front or rear wheels can be driven, but additional toothed belts can be used to transfer drive to the remaining wheels; 3. all wheels can be driven independently. In the case analyzed in this paper, the toothed belts were removed, and independent drive of all wheels was used.

In the case of the robot moving on soft ground, double wheels were used because the use of standard-width wheels resulted in too much wheels' sinkage on sand, making the robot unable to move. The following designations of geometric parameters of the robot were introduced in Figure 1b: L – wheelbase, W – track width ($A_1A_3 = A_2A_4 = L$, $A_1A_2 = A_3A_4 = W$), r_i, b_i – respectively radius, and width of the i-th wheel, where $i = 1, \ldots, 4$.

The velocity of the point R of the robot was assumed as the given parameter of the robot's motion, that is ${}^{O}v_{Rd} = {}^{O}v_{Rxd}$. The left superscript O means that the desired velocity is expressed in the stationary coordinates system. If the robot is in longitudinal motion, the velocities of the geometric centers of the wheels are equal to the velocity of point R, i.e., ${}^{O}v_{Ai} = {}^{O}v_{Aix} = {}^{O}v_{Rd}$.

With regard to desired angular velocities of wheel spins ω_{id}, if the robot moves without slip, they can be determined by solving the inverse kinematics problem for the mobile platform, that is, from the relationship:

$$\omega_{id} = \dot{\theta}_{id} = {}^{O}v_{Rd}/r_i. \tag{1}$$

a)

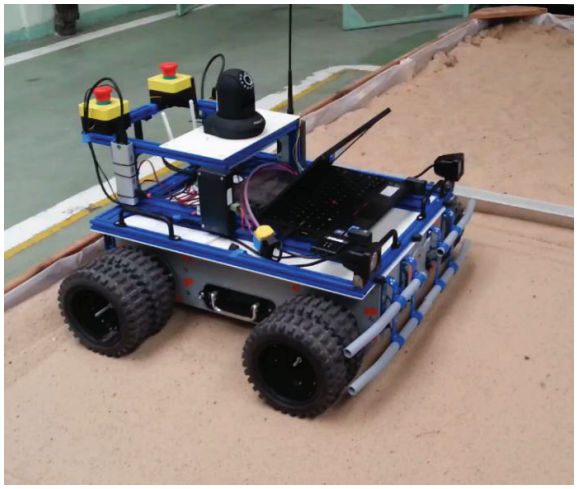

b)

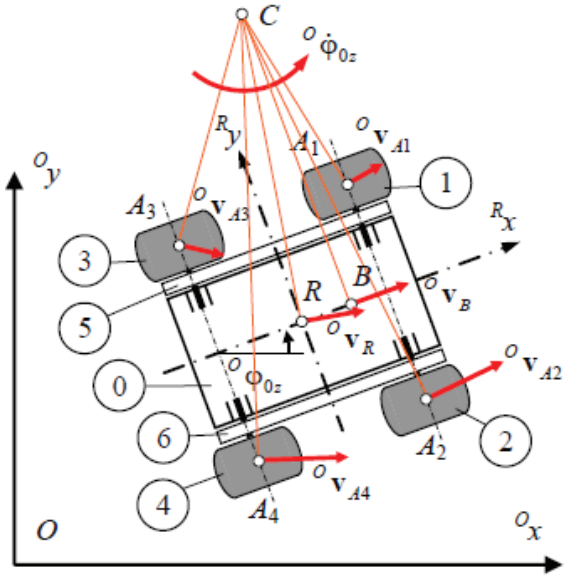

Figure 1. PIAP GRANITE robot during tests in a container filled with sand (a), kinematic structure of the robot (b)

However, wheel slippage may occur while the robot is moving. The measures of that slippage are instantaneous longitudinal slip ratios λ_i and mean longitudinal slip ratio λ_R (longitudinal slip ratio of the whole robot).

Those slip ratios are given with the formulas:

$$\lambda_i = \begin{cases} 0 & \text{for } v_{oi} = 0, \\ (v_{oi} - {}^{R}v_{Aix})/v_{oi} & \text{otherwise,} \end{cases} \tag{2}$$

$$\lambda_R = (s_{Rxd} - s_{Rx})/s_{Rxd}, \tag{3}$$

where: $v_{oi} = \omega_i r_i$ – wheel circumferential velocity, s_{Rx} – distance traversed by point R of the robot in longitudinal direction, s_{Rxd} – desired distance traveled by point R when rolling without slip.

For the present investigations, the following assumptions are adopted:

- wheels are treated as rigid bodies,
- the so-called multi-pass effect (in which a following wheel is subject to smaller rolling resistance, because it moves in a rut made by a leading wheel) are not considered,
- tread blocks of tires are neglected.

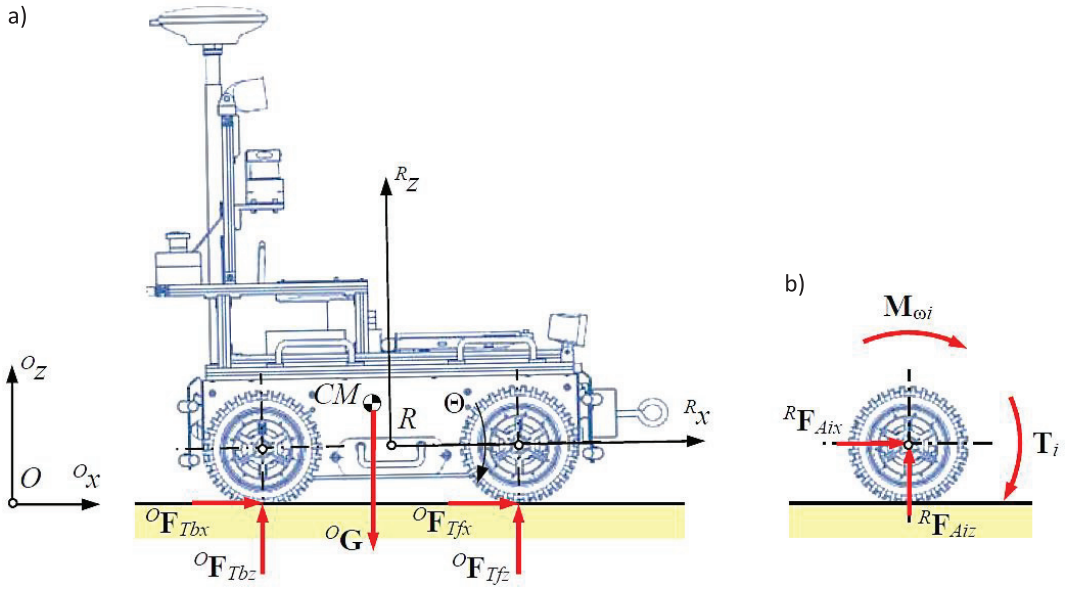

Figure 2. Illustration of forces and moments of force acting on the robot and its wheels

A multi-body dynamics model was derived for the robot. It was assumed that on the robot act the ground reaction forces, i.e., ${}^R\mathbf{F}_{Ti} = [{}^RF_{Tix}, {}^RF_{Tiy}, {}^RF_{Tiz}]^T$ $(i = 1, \dots, 4)$ and gravity force ${}^R\mathbf{G} = m_R{}^R\mathbf{g}$ (Fig. 2a), where m_R is robot total mass, ${}^R\mathbf{g} = [{}^Rg_x, {}^Rg_y, {}^Rg_z]^T$ the vector of gravity acceleration, and the left superscript R means that mentioned vectors are expressed in the moving coordinate system attached to the robot.

The following indexes are introduced for individual pairs of wheels: f – front wheels $(f = 1, 2)$, b – rear wheels $(b = 3, 4)$. On each wheel, apart from force of gravity and forces following from the interaction with the ground, act driving torque ${}^R\mathbf{T}_i = [0, T_i, 0]^T$ and moment of motion resistance ${}^R\mathbf{M}_{\omega i} = [0, M_{\omega i}, 0]^T$ (Fig. 2b).

As a result of the reduction of forces ${}^R\mathbf{F}_{Ti}$ to the axes of rotation of wheels, the forces ${}^R\mathbf{F}_{Ai} = {}^R\mathbf{F}_{Ti} = [{}^RF_{Aix}, {}^RF_{Aiy}, {}^RF_{Aiz}]^T$ are obtained.

The multi-body dynamics model is based on the following equations of dynamics for the whole vehicle and for individual wheels (associated with their spin):

$$m_R{}^Ra_{CMx} = \sum_{i=1}^{4} {}^RF_{Aix} + m_Rg\sin\Theta, \tag{4}$$

$$m_R{}^Ra_{CMz} = \sum_{i=1}^{4} {}^RF_{Aiz} - m_Rg\cos\Theta, \tag{5}$$

$$I_{CMy}\ddot{\Theta} = -\sum_{i=1}^{4} {}^RF_{Aix}{}^Rz_{CM} - \sum_{i=1}^{4} {}^RF_{Aiz}{}^Rx_i, \tag{6}$$

$$I_{Wiy}\ddot{\theta}_i = T_i + M_{\omega i}, \tag{7}$$

where: ${}^Rx_f = L/2 - {}^Rx_{CM}$, ${}^Rx_b = -L/2 - {}^Rx_{CM}$, ${}^Rx_{CM}$ and ${}^Rz_{CM}$ – robot mass center coordinates, I_{CMy} – robot mass moment of inertia about the axis parallel to ${}^Ry$ and passing through robot mass center, I_{Wiy} – wheel mass moment of inertia about its spin axis, $\mathrm{E} = \ddot{\Theta}$ and $\varepsilon_i = \ddot{\theta}_i$ – angular accelerations of rotation of respectively mobile platform and wheel about mentioned axes, ${}^Ra_{CMx}$ and ${}^Ra_{CMz}$ – component of the linear acceleration of the robot mass center.

The developed model enables the solution of the forward dynamics problem for the robot. According to this model, in a single time step of simulation, the following quantities are determined:

1) Instantaneous slip ratios for wheels λ_i $(i = 1, \dots, 4)$ and for the robot λ_R from equations (2) and (3).
2) Geometric quantities like maximum wheel sinkage z_{0i} and angles of wheel-terrain contact ϑ_{1i} and $\vartheta_{2i} = k_{\vartheta 2}\vartheta_{1i}$ (Fig. 3a).
3) Soil shear deformation $j_i(\vartheta_{1i})$ according to [13] and wheel sinkage $z_i(\vartheta_{1i})$ in the range of wheel-terrain contact angles from $-\vartheta_{2i}$ to ϑ_{1i} based on dependencies:

$$j_i(\vartheta_i) = r_i((\vartheta_{1i} - \vartheta_i) - (1 - \lambda_i)(\sin\vartheta_{1i} - \sin\vartheta_i)), \tag{8}$$

$$z_i(\vartheta_i) = \max(z_{0i} - r_i(1 - \cos\vartheta_i), 0). \tag{9}$$

4) Pressure $p_i(\vartheta_{1i})$ according to Bekker [11]:

$$p_i(\vartheta_i) = k(z_i(\vartheta_i))^n = \left(\frac{k_c}{b_i} + k_\varphi\right)(z_i(\vartheta_i))^n, \tag{10}$$

where: $k_c(k_\varphi)$ – cohesive (frictional) modulus of terrain deformation, n – terrain deformation exponent.

5) Normal stress $\sigma_i(\vartheta_{1i}) \approx p_i(\vartheta_{1i})$, maximum shear stress $\tau_{imax}(\vartheta_{1i})$, based on modified Mohr-Coulomb failure criteria [18] (Fig. 3b) including the case of moving tire surface with respect to soil:

$$\tau_{imax}(\vartheta_i) = \min(\mu_s\sigma_i(\vartheta_i), \quad c + \sigma_i(\vartheta_i)\tan\varphi), \tag{11}$$

that is taking into account soil cohesion c, internal friction angle φ and coefficient of static friction μ_s for the wheel-terrain pair according to [19].

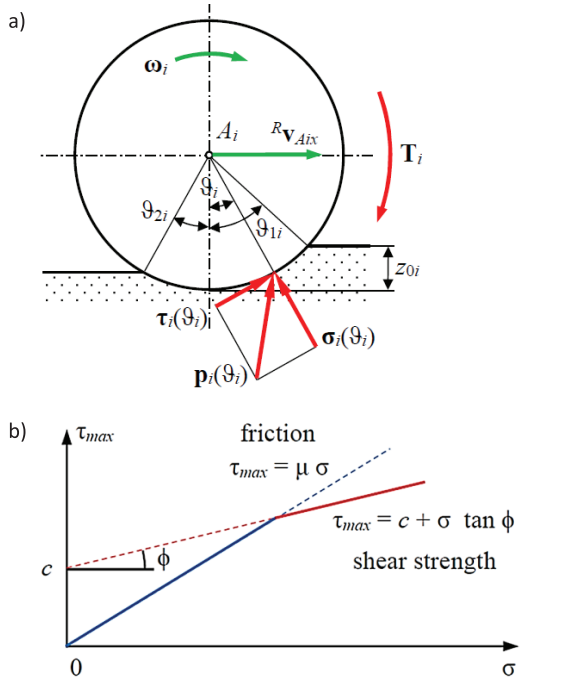

Figure 3. Model of an interaction of the wheel with deformable ground (a), $\tau_{max}(\sigma)$ dependency according to [13] (b)

6) Shear stresses according to Janosi-Hanamoto hypothesis [12] in the range of wheel-terrain contact angles from $-\vartheta_{2i}$ to ϑ_{1i}:

$$\tau_i(\vartheta_i) = \tau_{imax}(\vartheta_i)\left(1 - \exp\left(\frac{-j_i(\vartheta_i)}{K}\right)\right), \quad (12)$$

where K is the shear deformation parameter.

7) Forces and moments of force like: static normal load W_i, traction force F_i, motion resistance force R_{ti} and moment of motion resistance $M_{\omega i}$ based on the known stress distribution over wheel circumference, according to formulas in [13], i.e., based on equations:

$$W_i = br\int_{-\vartheta_{2i}}^{\vartheta_{1i}} w_i(\vartheta_i)\mathrm{d}\vartheta_i = b_i r_i \int_{-\vartheta_{2i}}^{\vartheta_{1i}} (\sigma_i(\vartheta_i)\cos\vartheta_i + \tau_i(\vartheta_i)\sin\vartheta_i)\mathrm{d}\vartheta_i, \quad (13)$$

$$F_i = b_i r_i \int_{-\vartheta_{2i}}^{\vartheta_{1i}} f_i(\vartheta_i)\mathrm{d}\vartheta_i = b_i r_i \int_{-\vartheta_{2i}}^{\vartheta_{1i}} \tau_i(\vartheta_i)\cos\vartheta_i\,\mathrm{d}\vartheta_i, \quad (14)$$

$$R_{ti} = b_i r_i \int_{-\vartheta_{2i}}^{\vartheta_{1i}} r_{ti}(\vartheta_i)\mathrm{d}\vartheta_i = b_i r_i \int_{-\vartheta_{2i}}^{\vartheta_{1i}} \sigma_i(\vartheta_i)\sin\vartheta_i\mathrm{d}\vartheta_i, \quad (15)$$

$$M_{\omega i} = -b_i (r_i)^2 \int_{-\vartheta_{2i}}^{\vartheta_{1i}} \tau_i(\vartheta_i)\mathrm{d}\vartheta_i, \quad (16)$$

and finally, resultant forces: longitudinal ${}^R F_{Tix} = F_i + R_{ti}$ and normal ${}^R F_{Tiz} = W_i + F_{ci}$, which includes component force resulting from the tire-ground system damping $F_{ci} = c_{ti}\dot{z}_{0i}\mathrm{sgn}(z_{0i})$.

8) Linear and angular accelerations, i.e.: ${}^R a_{CMx}$, ${}^R a_{CMz}$, $\ddot{\Theta}$ and $\ddot{\theta}_i$ $(i = 1, \ldots, 4)$, for the multi-body system of the robot based on the equations of dynamics (4)–(7).

It should be noted, that velocities v_{oi}, ${}^R v_{Aix}$, ω_i necessary for determination of slip ratios λ_i and λ_R in the first stage of the algorithm described above, coordinates of centers of wheels necessary for calculation of wheels' sinkage z_{0i} and angles ϑ_{1i} and ϑ_{2i} in the second stage of that algorithm are taken from the previous time step of calculations.

3. Results of Numerical Studies

Numerical studies were conducted in the Matlab/Simulink environment.

As part of the preliminary simulation tests, a numerical verification of the wheel-ground interaction model was carried out. In these studies, the previously mentioned parameters of this model were taken into account.

In the calculations, it was assumed that the change of the angle $\vartheta_i \in \langle -\vartheta_{2i}, \vartheta_{1i}\rangle$ will be implemented with a step $\Delta\vartheta = \pi/180$ rad. Moreover, it was assumed that $\vartheta_{2i} = k_{\vartheta_2}\vartheta_{1i}$, where $k_{\vartheta_2} = 0.4$. Calculations were performed for the following input data: ${}^R z_{Ai} = 0.0815$ m, ${}^R v_{Aix} = 1$ m/s, $\omega_i = 14$ rad/s, $T_i = 1$ Nm. The assumed angular velocity of the wheels is the maximum for the GRANITE robot and corresponds to the circumferential velocity equal to $v_{oi} = 1.4$ m/s.

Figure 4 shows the stress distributions $\boldsymbol{\sigma}_i(\vartheta_i)$ and $\boldsymbol{\tau}_i(\vartheta_i)$ on the wheel circumference, the resulting forces ${}^R F_{Aix}$, ${}^R F_{Aiz}$ and moment of force $\mathbf{M}_{\omega i}$ as well as the input and output data for the analyzed test.

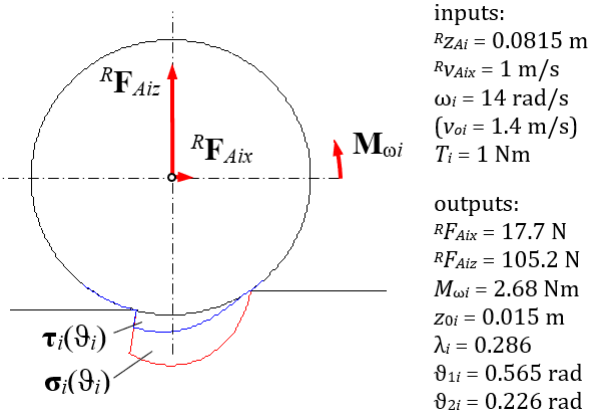

Figure 4. Illustration of the distribution of stresses $\boldsymbol{\sigma}_i(\vartheta_i)$ and $\boldsymbol{\tau}_i(\vartheta_i)$ on the wheel circumference as well as the resulting forces ${}^R\mathbf{F}_{Aix}$, ${}^R\mathbf{F}_{Aiz}$ and moment of force $\mathbf{M}_{\omega i}$

It should be noted that the obtained value of the ground normal reaction force is equal to ${}^{R}F_{Aiz} = 105.2$ N. In the case of the analyzed tire, such a force would cause its radial deformation equal to $\Delta r_i = 0.0026$ m, which is small in comparison with the maximum ground deformation $z_{0i} = 0.015$ m.

In turn, Figure 5 presents distributions of deformations of the ground and stresses on the wheel circumference as a function of the angle ϑ_i for the analyzed case.

According to the previously given formulas, after integration of stresses $\mathbf{w}_i(\vartheta_i)$, $\mathbf{r}_{ti}(\vartheta_i)$, $\mathbf{f}_i(\vartheta_i)$, $\mathbf{f}_{di}(\vartheta_i)$ and $\boldsymbol{\tau}_i(\vartheta_i)$, the resultant forces and moment of force, are obtained, i.e.: $\mathbf{W}_i$, $\mathbf{R}_{ti}$, $\mathbf{F}_i$, $\mathbf{F}_{di}$ and $\mathbf{M}_{\omega i}$.

It can be noticed that the value of the force $\mathbf{F}_{di}$ is significantly influenced by the stress distribution in the rear part of the tire in relation to the direction of movement.

In particular, stress $\mathbf{r}_{ti}(\vartheta_i)$ has negative values in the range $\vartheta_i \in (0, \vartheta_{1i})$ whilst positive values in the range $\vartheta_i \in (-\vartheta_{2i}, 0)$, while stress $\mathbf{f}_i(\vartheta_i)$ has positive values in the range $\vartheta_i \in (-\vartheta_{2i}, \vartheta_{1i})$, with the largest in the range $\vartheta_i \in (-\vartheta_{2i}, 0)$.

As part of the main simulation studies for the entire robot, the longitudinal motion for desired maximum velocities v_{Ru} from 0.2 m/s to 0.7 m/s was analyzed. Desired maximum acceleration a_{Rmax} during speeding up and braking, as well as desired total distance L_p to be traveled were chosen individually for the particular case of motion. Desired parameters of robot motion are summarized in Table 1.

The values of the basic parameters of the PIAP GRANITE mobile robot used in simulation studies are shown in Table 2. Soil parameters required by the adopted model and based on work [14] are presented in Table 3.

The aggregated results of the research are shown in Figure 6. It can be noticed that the smallest slip ratios are for dry sand and the largest for sandy loam and that the slip ratios increase with desired velocity. The largest wheel sinkage occurs for dry sand, and for the other analyzed grounds, it is much smaller. The wheel sinkage increases slightly with robot velocity.

In the case of dry sand, wheel sinkage is much larger in comparison to radial deformation of the tire, which would occur on rigid ground. Tire radial deformation would be 2–3 mm because the radial stiffness of the tire is $k_{ri} = 40,000$ N/m [17]. For the remaining types of ground, wheel sinkage is of comparable order to this deformation. The driving torques increase with velocity, i.e., torques increase nearly two times when comparing results for 0.2 m/s and 0.7 m/s cases of desired robot velocity.

In Figures 7–10, detailed results for robot motion with desired velocity ${}^{R}v_{Rd} = 0.5$ m/s on dry sand, sandy loam and clayey soil are illustrated.

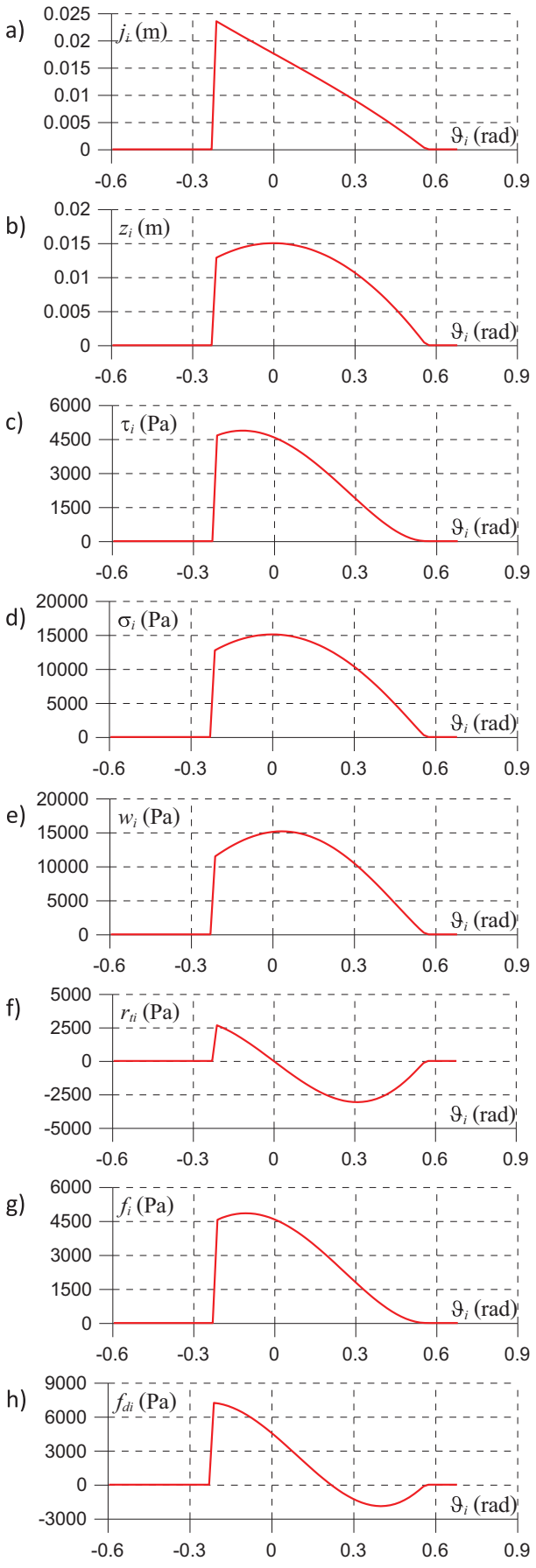

Figure 5. Distributions on the wheel circumference of soil deformations: tangential $j_i(\vartheta_i)$ (a) and normal $z_i(\vartheta_i)$ (b), as well as stresses resulting from them: tangential $\boldsymbol{\tau}_i(\vartheta_i)$ (c), normal $\boldsymbol{\sigma}_i(\vartheta_i)$ (d) and resultants: $\mathbf{w}_i(\vartheta_i)$, $\mathbf{r}_{ti}(\vartheta_i)$, $\mathbf{f}_i(\vartheta_i)$, $\mathbf{f}_{di}(\vartheta_i) = \mathbf{r}_{ti}(\vartheta_i) + \mathbf{f}_i(\vartheta_i)$ (e–h)

Table 1. Desired robot motion parameters for the investigated cases

v_{Ru} (m/s)	0.2	0.3	0.5	0.7
a_{Rmax} (m/s^2)	0.6	1.2	1.2	2.4
L_p (m)	1.0	2.0	2.5	3.0

Table 2. Basic parameters of the PIAP GRANITE mobile robot used in simulation studies

Dimensions	$L = 0.425$ m, $W = 0.59$ m, $r_i = 0.0965$ m, $b_i = 2 \cdot 0.064$ m
Masses of the bodies	$m_0 = 36.54$ kg, $m_i = 1.64$ kg
Robot mass center coordinates	${}^R x_{CM} = -0.012$ m, ${}^R y_{CM} \approx 0$ m, ${}^R z_{CM} = 0.06$ m
Mass moments of inertia	$I_{Wy} = 0.016$ kg m^2, $I_{CMy} = 0.51$ kg m^2
Tire parameters	$k_{ri} = 40\,000$ N/m, $c_{ti} = 1000$ Ns/m

Table 3. Soil parameters assumed for the research [14]

	Dry sand	Sandy loam	Clayey soil
n(-)	1.1	0.7	0.5
k_c (kN/m^{n+1})	0.9	5.3	13.2
k_φ (kN/m^{n+2})	1 523	1 515	692
c (kPa)	1	1.7	4.14
φ (deg)	30	29	13
K (m)	0.025	0.025	0.01

In particular in Figure 7, time histories of desired and actual robot velocities as well as circumferential velocity resulting from wheel spin are presented. It can be noticed that during steady motion, value of the actual robot velocity ${}^R v_{Rx}$ is noticeably smaller with respect to desired velocity ${}^R v_{Rd}$. This is because the robot does not achieve the desired acceleration, especially in the initial stage of movement.

This, in turn, results from the high values of the longitudinal slip ratios of the wheels λ_i occurring especially during the acceleration of the robot. The robot's actual longitudinal velocity ${}^R v_{Rx}$ is closest to the desired velocity ${}^R v_{Rd}$ for the case of the robot moving on dry sand. In all cases, it can be seen that the maximum circumferential velocity of wheels v_o is reached with a delay, which results from the inclusion of the dynamics of the drive units in the model, described in paper [17].

In Figures 8–9 the time histories of longitudinal slip ratios and sinkage for front and rear wheels are shown, respectively. The time histories of longitudinal slip ratios are similar for front and rear wheels. However, a difference can be noticed in the case of wheels' sinkage, due to the fact that the center of mass is located in the rear part of the vehicle. For this reason, higher values are obtained for the rear wheels. Similar to the velocity, the time histories of the longitudinal slip ratios are similar to each other for the

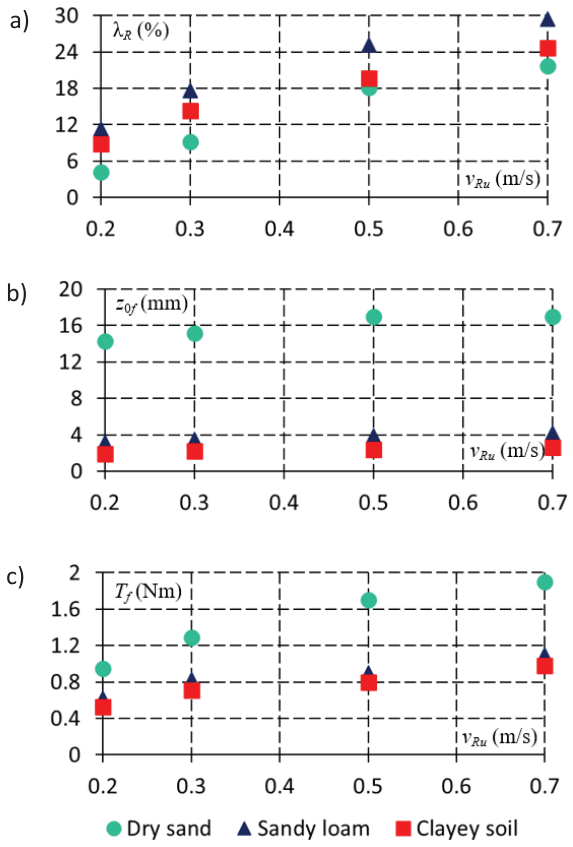

Figure 6. Influence of type of soil and desired motion velocity on: longitudinal slip ratios for the robot (a), wheel sinkage (b), driving torques (c)

analyzed ground cases, but during acceleration they are apparently the smallest for the movement on dry sand. However, there are large differences in the time histories of wheels' sinkage for the analyzed types of the ground. Definitely the highest values of wheels' sinkage occur for the robot's movement on dry sand. In turn, the smallest values can be seen in the case of clayey soil.

Finally, in Figure 10, the time histories of driving torques for front and rear wheels are illustrated. During acceleration, the highest values of driving torques are achieved when the robot moves on dry sand. In the case of other grounds, similar results were obtained, moreover, the drive torques for the front and rear road wheels are less differentiated in relation to the movement on dry sand.

Simulation studies were also carried out to analyze the impact of wheel geometric parameters on longitudinal slip ratios, wheel sinkage and driving torques.

In this research, in relation to standard configuration of the robot, the following wheel solutions were analyzed:

1) wheels with width reduced by 50%,
2) wheels with a diameter increased by 50%.

The results of simulation research indicate that for the analyzed robot motion velocities, changing the geometric parameters of the wheels has a small impact on the driving torques.

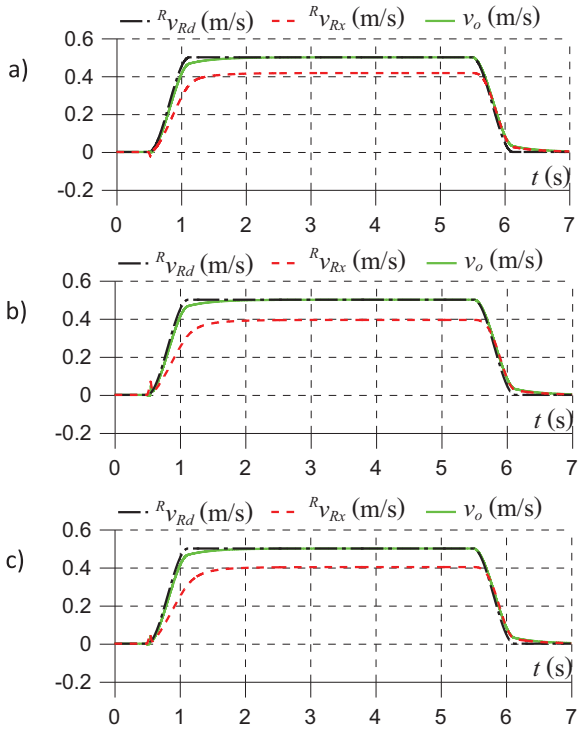

Figure 7. Time histories of desired velocity $^{R}v_{Rd}$ and actual velocity $^{R}v_{Rx}$ of the robot as well as circumferential velocity of wheels v_o obtained in simulation of the robot's movement with the maximum velocity $v_{Ru} = 0.5$ m/s on: dry sand (a), sandy loam (b) and clayey soil (c)

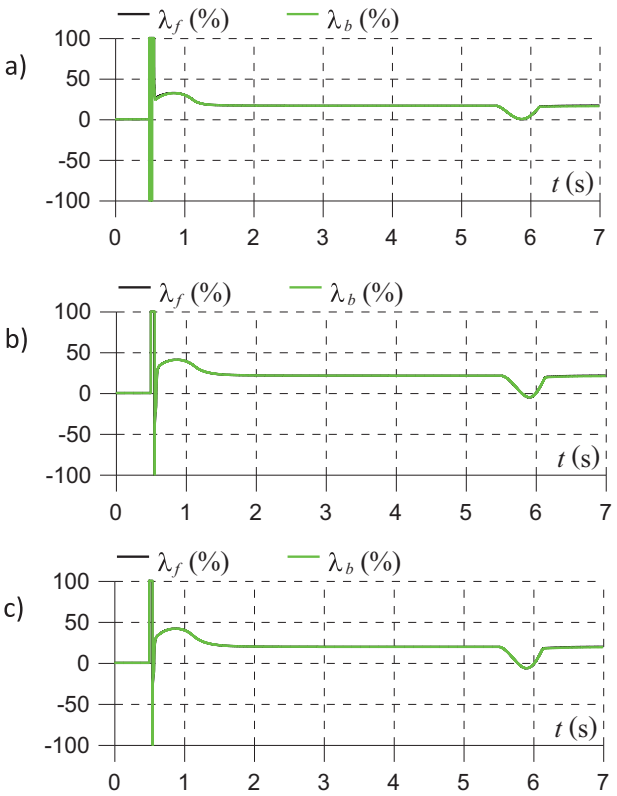

Figure 8. Time histories of longitudinal slip ratios for front and rear wheels obtained in simulation of the robot's movement with the maximum velocity $v_{Ru} = 0.5$ m/s on: dry sand (a), sandy loam (b) and clayey soil (c)

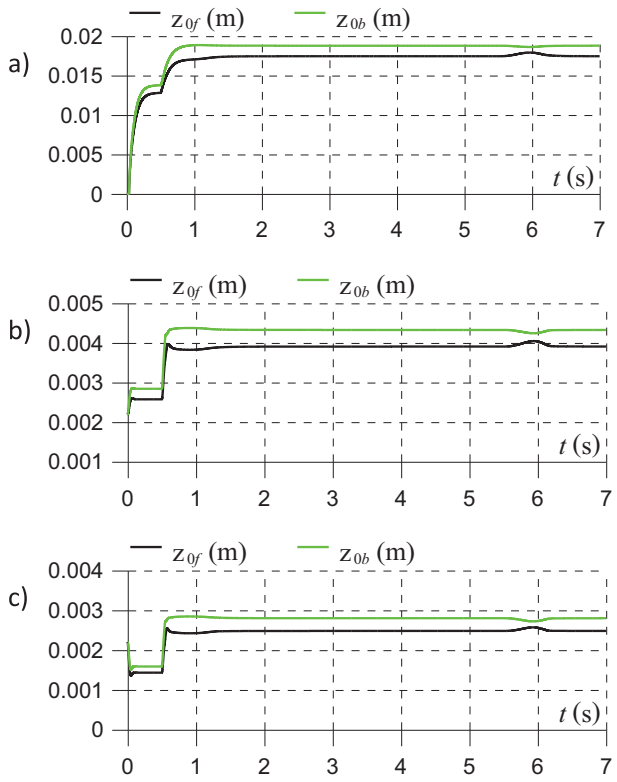

Figure 9. Time histories of sinkage for front and rear wheels obtained in simulation of the robot's movement with the maximum velocity $v_{Ru} = 0.5$ m/s on: dry sand (a), sandy loam (b) and clayey soil (c)

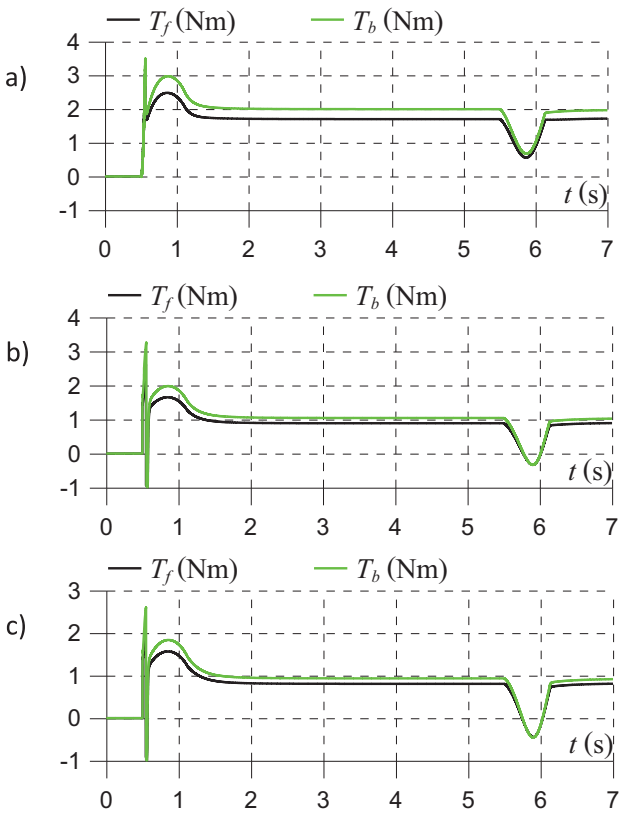

Figure 10. Time histories of driving torques for front and rear wheels obtained in simulation of the robot's movement with the maximum velocity $v_{Ru} = 0.5$ m/s on: dry sand (a), sandy loam (b) and clayey soil (c)

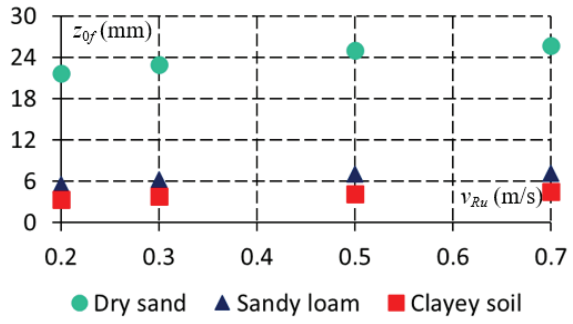

Figure 11. Influence of type of soil and desired motion velocity on wheel sinkage for wheels with width reduced by 50%

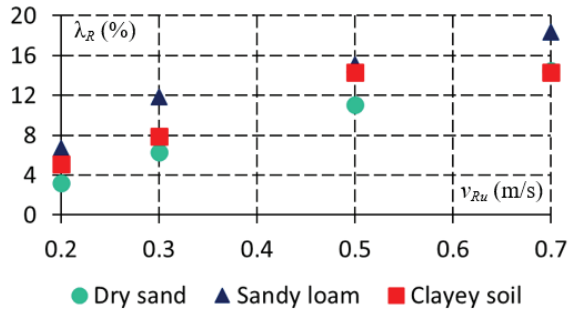

Figure 12. Influence of type of soil and desired motion velocity on longitudinal slip ratios for the robot for wheels with a diameter increased by 50%

When wheels with a smaller width were used, slight changes in longitudinal slip ratios and a significant increase in wheel sinkage were observed. The change in wheel sinkage can be seen from the comparison of the results shown in Figure 6b for wheels with a larger width and in Figure 11 for wheels with a smaller width. This observation is consistent with the effects of preliminary experimental tests for the PIAP GRANITE robot and was the reason for the use of wheels with larger width.

The results of simulation studies also indicate that the use of wheels with a diameter 50% larger leads to a reduction in wheel sinkage, but this change is not significant. However, the use of larger diameter wheels leads to a significant reduction in longitudinal slip ratios, especially at higher velocities. This can be seen by comparing the results shown in Figure 6a for wheels with a smaller diameter with the results in Figure 12 for wheels with a 50% larger diameter.

4. Conclusion and Future Works

Within this paper the simulation studies of influence of type of deformable ground on longitudinal motion of lightweight wheeled robot was carried out.

Investigated cases included four desired velocities of motion, i.e.: 0.2 m/s, 0.3 m/s, 0.5 m/s and 0.7 m/s and three types of ground: dry sand, sandy loam and clayey soil.

For all those cases, aggregated results of wheel slip ratio, wheel sinkage and wheel driving torque were presented. Detailed results for the case of 0.5 m/s velocity on all analyzed types of soil were also shown.

The following main conclusions can be drawn from the conducted numerical research.

If a lightweight wheeled mobile robot moves on a deformable ground, then:

- longitudinal slip ratio significantly increases with desired velocity;
- wheel sinkage increases with desired velocity – in case of motion on dry sand, wheel sinkage is much larger than radial deformation of tire which would occur for comparable wheel load on rigid ground;
- wheel driving torques increase with velocity and reach the largest values for robot motion on dry sand;
- changing the wheel width significantly affects wheel sinkage, i.e., it is higher for narrower wheels;
- changing the wheel diameter causes, in turn, a change in the longitudinal slip ratios, i.e., they decrease as the wheel diameter increases.

The scope of further research may include:

- modeling the dynamics of both lightweight and heavy vehicles using wheels with fillings of various mechanical properties;
- simulation studies taking into account tire deformation, tread blocks and multi-pass effect in tire model;
- experimental studies of the robot motion on sandy loam and clayey soil;
- simulation and experimental studies of robot turning and rotation in place for various types of the ground.

AUTHORS

Maciej Trojnacki* – Warsaw University of Technology, Faculty of Mechatronics, Institute of Micromechanics and Photonics, Boboli 8, 02-525 Warsaw, Poland, e-mail: maciej.trojnacki@pw.edu.pl.

Przemysław Dąbek – ŁUKASIEWICZ Research Network—Industrial Research Institute for Automation and Measurements PIAP, Al. Jerozolimskie 202, 02-486 Warsaw, Poland, e-mail: przemyslaw.dabek@piap.lukasiewicz.gov.pl.

*Corresponding author

References

[1] K. Zhou, S. Lei, and X. Du. "Modelling and dynamic analysis of slippage level for large-scale skid-steered unmanned ground vehicle," *Sci Rep*, vol. 12, no. 1, Art. no. 1, Sep. 2022, doi: 10.1038/s41598-022-20262-z.

[2] J. Guo, H. Gao, L. Ding, T. Guo, and Z. Deng. "Linear normal stress under a wheel in skid for wheeled mobile robots running on sandy terrain," *Journal of Terramechanics*, vol. 70, pp. 49–57, Apr. 2017, doi: 10.1016/j.jterra.2017.01.004.

[3] M. Ciszewski, M. Giergiel, T. Buratowski, and P. Małka, *Modeling and Control of a Tracked Mobile*

Robot for Pipeline Inspection. Springer Nature, 2020.

[4] L. Liang et al. "Model-Based Coordinated Trajectory Tracking Control of Skid-Steer Mobile Robot with Timing-Belt Servo System," *Electronics*, vol. 12, no. 3, Art. no. 3, Jan. 2023, doi: 10.3390/electronics12030699.

[5] A. J. Moshayedi, A. S. Roy, S. K. Sambo, Y. Zhong, and L. Liao. "Review On: The Service Robot Mathematical Model," *EAI Endorsed Transactions on AI and Robotics*, vol. 1, pp. e8–e8, Feb. 2022, doi: 10.4108/airo.v1i.20.

[6] K. Peng, X. Ruan, and G. Zuo. "Dynamic model and balancing control for two-wheeled self-balancing mobile robot on the slopes," in *Proceedings of the 10th World Congress on Intelligent Control and Automation*, Jul. 2012, pp. 3681–3685. doi: 10.1109/WCICA.2012.6359086.

[7] P. Lichota. "Wavelet Transform-Based Aircraft System Identification," *Journal of Guidance, Control, and Dynamics*, vol. 46, no. 2, pp. 350–361, Feb. 2023, doi: 10.2514/1.G006654.

[8] S. Sutulo and C. Guedes Soares. "An algorithm for offline identification of ship manoeuvring mathematical models from free-running tests," *Ocean Engineering*, vol. 79, pp. 10–25, Mar. 2014, doi: 10.1016/j.oceaneng.2014.01.007.

[9] J. Giergiel, K. Kurc, and D. Szybicki. "Identification of the Mathematical Model of an Underwater Robot Using Artificial Inteligence," *Mechanics and Mechanical Engineering*, 2014, Accessed: Jan. 16, 2024. [Online]. Available: https://www.semanticscholar.org/paper/Identification-of-the-Mathematical-Model-of-an-Giergiel-Kurc/5b4cfa76e8916013fa613c40ff06d3a966542853.

[10] A. Perrusquía and W. Yu. "Identification and optimal control of nonlinear systems using recurrent neural networks and reinforcement learning: An overview," *Neurocomputing*, vol. 438, pp. 145–154, May 2021, doi: 10.1016/j.neucom.2021.01.096.

[11] M. G. Bekker, *Off-the-road Locomotion: Research and Development in Terramechanics*. University of Michigan Press, 1960.

[12] J. Y. Wong, *Theory of Ground Vehicles, 3rd Edition*, 3rd edition. New York: Wiley-Interscience, 2001.

[13] Sh. Taheri, C. Sandu, S. Taheri, E. Pinto, and D. Gorsich. "A technical survey on Terramechanics models for tire–terrain interaction used in modeling and simulation of wheeled vehicles," *Journal of Terramechanics*, vol. 57, pp. 1–22, Feb. 2015, doi: 10.1016/j.jterra.2014.08.003.

[14] K. Iagnemma and S. Dubowsky, *Mobile Robots in Rough Terrain: Estimation, Motion Planning, and Control with Application to Planetary Rovers*. Springer, 2004.

[15] L. Ding, H. Gao, Z. Deng, K. Yoshida, and K. Nagatani. "Slip ratio for lugged wheel of planetary rover in deformable soil: definition and estimation," in *2009 IEEE/RSJ International Conference on Intelligent Robots and Systems*, Oct. 2009, pp. 3343–3348. doi: 10.1109/IROS.2009.5354565.

[16] Z. Wang et al. "Wheels' performance of Mars exploration rovers: Experimental study from the perspective of terramechanics and structural mechanics," *Journal of Terramechanics*, vol. 92, pp. 23–42, Dec. 2020, doi: 10.1016/j.jterra.2020.09.003.

[17] M. Trojnacki and P. Dąbek. "Studies of dynamics of a lightweight wheeled mobile robot during longitudinal motion on soft ground," *Mechanics Research Communications*, vol. 82, pp. 36–42, Jun. 2017, doi: 10.1016/j.mechrescom.2016.11.001.

[18] G. N. B. Hathorn, K. Blackburn, and J. L. Brighton. "An Investigation into Wheel Sinkage on Soft Sand," *Tire Science and Technology*, vol. 42, no. 2, pp. 85–100, Apr. 2014, doi: 10.2346/tire.14.420201.

[19] "Tire friction and rolling coefficients," HP Wizard. Accessed: Jul. 25, 2023. [Online]. Available: https://hpwizard.com/tire-friction-coefficient.html.